Materials Research
Express

INCLUSIVE PUBLISHING
TRUSTED SCIENCE

PURPOSE-LED
PUBLISHING™

PAPER

Plasmonic responses of metallic/dielectric core-shell nanoparticles on a dielectric substrate

To cite this article: Dilan Avşar *et al* 2019 *Mater. Res. Express* **6** 065006

View the article online for updates and enhancements.

You may also like

- Theoretical Study of Local Surface Plasmon Resonances on a Dielectric-Ag Core-Shell Nanosphere Using the Discrete-Dipole Approximation Method
Ye-Wan Ma, , Zhao-Wang Wu et al.
- Theoretical calculation of optical absorption property of Cu@Ag core–shell composite nanoparticle
Supachai Sompech, Sukhontip Thaomola, Artit Chingsungnoen et al.
- Calculated Optical Properties of Dielectric Shell Coated Gold Nanorods
Cao Min, Wang Meng and Gu Ning

kiutra

Millikelvin characterization for superconducting devices

L-TYPE RAPID

- **< 4 hrs** sample loading and cooldown to base
- **50 mK** base temperature
- **30 min** warm up and sample exchange

Find out more →



This content was downloaded from IP address 144.122.201.61 on 02/10/2026 at 04:08

Materials Research Express



RECEIVED
20 December 2018

REVISED
28 January 2019

ACCEPTED FOR PUBLICATION
18 February 2019

PUBLISHED
6 March 2019

PAPER

Plasmonic responses of metallic/dielectric core-shell nanoparticles on a dielectric substrate

Dilan Avşar[1], **Hakan Ertürk**[1] and **M Pınar Mengüç**[2]

[1] Department of Mechanical Engineering, Boğaziçi University, İstanbul, Turkey
[2] Center for Energy, Environment and Economy (CEEE), Özyeğin University, İstanbul, Turkey

E-mail: hakan.erturk@boun.edu.tr **and** pinar.menguc@ozyegin.edu.tr

Keywords: localized surface plasmon resonance, core-shell nanoparticles, hybridization of plasmonic response, discrete dipole approximation with surface interactions, surface evanescent waves, nano-manufacturing

Abstract

The effect of material selection on the plasmonic response and local absorption are evaluated for core–shell nanoparticles placed over a BK7 glass substrate. Eight different core–shell pairs are studied using the vectorized version of discrete dipole approximation with surface interactions (DDA-SI). Two classes of dielectric core-metallic shell and metallic core-dielectric shell particles are considered. It is shown that core–shell structures with dielectric materials can have absorption enhancement compared to the bare metallic nanoparticles. Moreover, it is observed that core–shell pairs yield multipeak localized surface plasmon resonance (LSPR) response due to their hybrid structure. Absorption enhancement and LSPR tuning ranges are shown with different dielectric materials that can be used in localized heating of designated core–shell NPs placed over a surface for nanomanufacturing purposes. In order to determine the optimum size configurations, a number of core–shell pairs are explored with specified volumetric filling ratio of core materials.

1. Introduction

Noble metals such as gold, silver, and copper, have always been the center of interest due to their unique plasmonic response. At nanoscales, after a critical length scale (i.e. Fermi wavelength, λ_f) is exceeded, oscillating charges on the surface of the nanoparticle are forced to resonate with the incident light frequency generating evanescent waves localized in the near-field. If an object is placed within few hundred nanometers, they engage in a near-field coupling resulting in EM field enhancement and increased absorption with localized heating. This phenomenon takes place where the resonance occurs at the highest level of field intensity and it is called as the localized surface plasmon resonance (LSPR) [1, 2].

There are numerous applications based on the optical response of the nanoparticles with their spectral absorption, scattering and extinction behavior at the LSPR wavelengths, including sensing with surface enhanced Raman spectroscopy (SERS) [3], near field optical microscopy (SNOM) [4], tip-enhanced Raman spectroscopy (TERS) [5], cancer therapies with photothermal ablation and targeted drug delivery [6, 7], imaging systems with contrast agents [8], and nano-manufacturing technologies [9, 10]. Selective and localized heating of nanoparticles are essential in both biomedical and nano-scale manufacturing applications. When the plasmonic particles are illuminated by an EM wave at a wavelength close to their LSPR wavelength, particles are heated. Then, they can be used not only to ablate the tumor tissue for photothermal therapies but also to tailor the surface by creating a deposit of molten nanoparticles for nano-manufacturing [6, 10, 11].

Hawes *et al* [12] analyzed the scattering and absorption profiles of nanosized particles on different substrates numerically and experimentally and determined the excitation behavior of particles with various particle separation distances. Their computational study showed that gold and silver nanocylinders placed on different surfaces such as glass, silver, and gold films have alternating absorption profiles under the illumination by total internal reflection (TIR) that creates surface decaying evanescent waves. The cases with the metal films resulted

© 2019 IOP Publishing Ltd

in less absorption by nanoparticles than the ones with the glass substrate. These results show the possibility of an effective design to heat the particles at their specific resonance wavelength [12].

Further studies show that local heating of gold nanoparticles on a dielectric glass substrate can be implemented with the exploitation of the surface plasmon resonance and near-field coupling of an atomic force microscope (AFM) positioned over the nanoparticles. In this configuration, transverse magnetic (TM) wave illumination is preferred for enhanced absorption efficiency due to additional perpendicular component of the evanescent wave from TM [2, 10, 13]. A numerical study for an array of gold nanoparticles on a glass substrate under an AFM tip shows that redshift of the plasmon resonance wavelength is observed with enhanced absorption when the separation distance of the particles were increased to an optimal value [13]. The study of complex nanostructures on a BK7 substrate also showed that gold array with combinations of cubical and spherical geometries can also provide a redshift of the plasmon resonance wavelength and greater absorption efficiency [14].

While these studies demonstrate the effects of near-field coupling and surface interactions on the field enhancement, other studies also report that hybrid structures of metal nanoparticles can have distinct optical responses than the bare metal nanoparticles [15]. Especially for selective heating applications, dielectric core with large refractive index can be used to alter the plasmonic response of the metallic particles [7, 11]. Other numerical and experimental studies also show that silica core with gold shell nanostructures can increase absorption with uniform heating [16] and have LSPR response in a range of visible (vis) to near-infrared (NIR) region of the spectrum [17].

The core–shell nanostructures have various advantages: the plasmonic response of the nanoparticles can be tuned and/or hybridized by changing the material composition, core/shell size ratio, and the surrounding medium. Core–shell nanoparticles can be classified as dielectric-metal, metal-dielectric, and metal-metal according to their material compositions for the core and shell, respectively. Such nanoparticles can have unprecedented ways to exploit their optical properties with optimum field enhancement and tunable LSPR response [8]. The hybrid structure of core–shell nanoparticles is promising for local heating applications that necessitate a detailed study of absorption mechanisms with material and size combinations.

One of the first experimental studies on core–shell nanoparticles was carried out by Zhou *et al* [15] with dielectric core-metal shell NPs. It was observed that shifting of the plasmon resonance to longer wavelengths was possible by varying gold shell thickness. Dielectric core-metal shell NPs are studied in optical contrast agents, targeted heat delivery, and photothermal ablation with their tunable LSPR wavelengths. The most advantageous optical response of the dielectric-metal core–shell nanoparticles is the redshift of plasmon peaks when the metal shell thickness is decreased. Therefore, dielectric-metal core–shell nanoparticles are good candidates for *in vivo* diagnosis of cancer tissues due to their optimum optical transmission through tissue within NIR region [17, 18]. Oldenburg *et al* [19] also showed that the optical resonance of silica core and gold shell NPs can be easily tuned from visible to mid-infrared wavelengths by increasing the core/shell ratio. Through numerical and experimental studies, similar conclusions have been reached with the dielectric core and noble metal shell nanoparticles [19, 20]. Dielectric-metal core–shell nanoparticles are also sensitive to the changes in the surrounding medium, where an increase of refractive index of the medium results in both redshift and increased intensity, facilitating their use in refractive index sensing applications [18, 21].

Dielectric coating of metal core provides chemical and physical stability of both the plasmonic core and the environment, while it can also prevent agglomeration of the particles [22, 23]. Metal-dielectric NPs can be used in photothermal therapy, biosensors, and solar cells with their enhanced plasmon resonance due to stronger Coulombic interactions between polarization charges of the dielectric shell and the free electrons in the plasmonic core as a result of the dielectric shell having larger refractive index than the core. This phenomenon has also been studied experimentally with gold core-silica shell for photothermal ablation techniques [24]. The numerical comparison of dielectric-metal and metal-dielectric core–shell nanoparticles has shown that gold core with silica shell has higher scattering/absorption ratio in NIR region, which is preferred in solar cell applications [23]. Moreover, studies have shown that contrary to dielectric-metal core–shell NPs, metal-dielectric ones have redshifted plasmon as the shell thickness increases while their absorption efficiency responses mostly depend on the volume of the NP and shielding effect of the dielectric shell [23].

Electromagnetic wave interactions with NPs and their resulting optical response can be studied numerically with the computational electromagnetic methods (CEM) through the solutions of Maxwell's equations. The discrete dipole approximation (DDA) is one of the semi-analytical CEM for which the nanoparticle is represented by a number of dipoles. Since the general formulation of DDA, developed by Purcell and Pennypacker [25], many open source DDA methods have been implemented such as DDSCAT written in FORTRAN [26, 27], and ADDA written in C++ [28]. Another open source MATLAB™ toolbox, DDA with surface interactions (DDA-SI), was developed by Loke and Mengüç [29] for the objects placed on a dielectric surface. The toolbox is validated against microwave analog experiments, and other discretization methods for particles on a surface [30, 31]. This method was then further improved with the vectorized version of DDA-SI

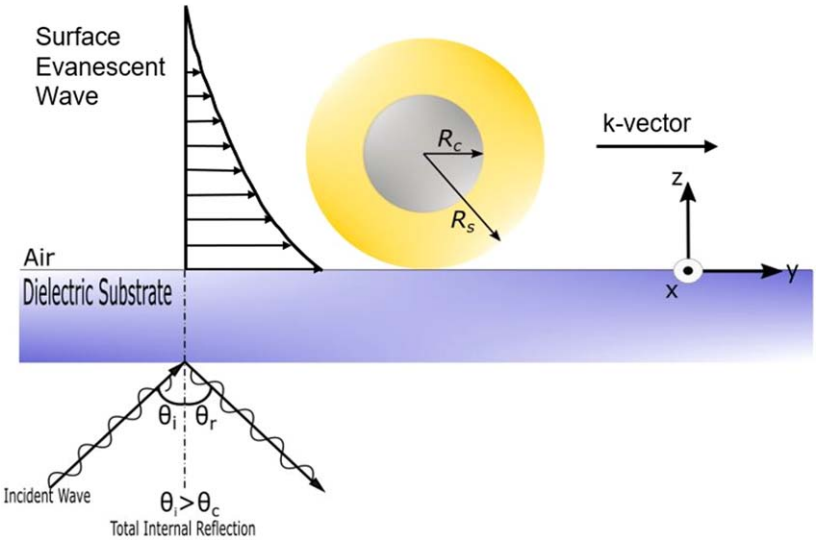


Figure 1. A schematic view of the configuration for single core–shell system being represented with core radius (R_c) and outer shell radius (R_s). TE-polarized wave is incident with an angle greater than the critical angle (θ_c) for TIR under the BK7 substrate that creates surface evanescent wave propagating and decaying in y- and z-directions, respectively.

(DDA-SI-v) by Talebi-Moghaddam *et al* [16]. Recently, for an accelerated calculation with more accuracy, Rostampour-Fathi *et al* developed the third version of DDA-SI toolbox (zDDA-SI) [14].

Although there are numerous numerical studies based on NPs and their LSPR response, most of them were analyzed within a free space without surface interactions or in an aggregate form. As stated earlier, numerical study of silica core-gold shell NP being placed on a BK7 substrate showed that enhanced absorption efficiency and a redshift of the plasmon response can be achieved for selective heating and nano-manufacturing purposes [16]. There are, however, limited number of studies on material comparisons that will guide the experimentalists to the optimum configurations for the enhanced effects. The objective of the present paper is to focus on the spectral absorption profiles of core–shell nanoparticles with various core–shell material and size configurations accompanied with surface interactions. Current study is the follow-up investigation of [16] with single core–shell nanoparticle placed on a semi-infinite BK7 glass substrate being illuminated by an EM light from bottom with total internal reflection. The spectral absorption behavior of core–shell nanoparticle is numerically studied with selected metal-dielectric, and dielectric-metal pairs for core and shell materials, respectively.

In this study, volumetric filling ratio of core material to the whole nanoparticle will be utilized to be able to set standards for size configurations. This ratio will be used for the comparisons of metal and dielectric pairs with their LSPR response and absorption efficiency. In this comparison study, numerical simulations are performed with DDA-SI-v for absorption efficiency calculations of core–shell NPs with at most 50 nm in diameter. This extensive study is expected to shed light on the material selections with their effects on the absorption efficiencies that can be useful for localized heating applications and nano-scale manufacturing.

2. Problem statement

The system consists of single core–shell NP, which is placed on a semi-infinite BK7 glass substrate in vacuum ($n = 1$). As shown in figure 1, an incident wave is illuminated from below the dielectric surface with an incident angle greater than the critical angle for total internal reflection (TIR) that results in surface evanescent waves interacting with the nanoparticle. Unlike the study in [16], TE-polarized (rather than TM-polarized) EM wave illumination in the wavelength range from 300 nm to 800 nm is considered. Since we do not consider any vertically placed AFM probe, it is not required to use TM wave for field enhancement. Moreover, the simulations with TM-polarization have the same LSPR wavelength responses with slight decrease in absorption efficiency values. Therefore, the results presented for TE waves are also representative of TM polarization cases. In the analysis, dielectric-metallic and metallic-dielectric core–shell pairs are used. Materials chosen include gold (Au) and silver (Ag) for metals, and Gallium phosphide (GaP) and Silicon dioxide (SiO_2) for dielectrics. GaP is chosen due to its imaginary part of the refractive index, k, being nonzero for the wavelengths smaller than 490 nm. Unlike in the case of SiO_2, GaP has real part of the refractive index, n, greater than 3 that can create field confinement in subwavelength volumes and broadband near-field response [32, 33].

Table 1. Core and shell sizes for FC and FNP cases with corresponding volumetric filling ratio (f_r) ranges.

NP type	Core diameter, D_c (nm)	Shell diameter, D_s (nm)	f_r Range
Fixed Core (FC)	20	22–50	0.751–0.064
	20	20	1
Fixed NP (FNP)	15–45	50	0.027–0.729
	50	50	1

The absorption efficiency calculations are carried out for both varying shell thickness with fixed core diameter ($D_c = 20$ nm) and varying core size with fixed NP diameter ($D_s = 50$ nm). LSPR response of the particle is investigated through both fixed core (FC) and fixed nanoparticle (FNP) sizes. Size configurations are then used for the comparisons based on the volumetric filling ratio (f_r), which is defined as the ratio of the core volume with radius (R_c) to the nanoparticle volume defined based on shell radius (R_s), $f_r = (R_c/R_s)^3$. The summary of size configurations are tabulated in table 1 with the corresponding f_r ranges.

For the simulations, refractive index of the core–shell nanoparticle materials are obtained from experimental measurements of [34] for Au and Ag while the data for GaP is used from [35]. For the optical properties of BK7 substrate and SiO_2, an empirical relation of refractive index and wavelength is used with Sellmeier equation.

3. Methodology

The spectral absorption efficiency calculations are carried out by using DDA with surface interactions (DDA-SI). As mentioned above, this toolbox is well established and further developed with the vectorized version of it (DDA-SI-v) [16]. Since the model is explained in detail in [29], the mathematical formulation of DDA-SI is not discussed here.

The DDA analysis through DDA-SI-v requires the use of adequate number of dipoles (N) for an accurate representation of each nanoparticle. The optimum dipole number is identified as 1472, where the predicted absorption efficiency values converge. The lattice spacing (d) criterion is also considered especially for the metals that have large imaginary part of the refractive index at long wavelengths after 500 nm [26]. The lattice spacings of each material being used for the simulations show that the minimum lattice spacing is $d_{\min} = 5.57$ nm for GaP with refractive index of $3.75 + 2.06i$ at 300 nm wavelength. The number of dipoles is selected larger than the one required for the minimum lattice spacing. Corresponding lattice spacings of the nanoparticles are then calculated based on nanoparticle volume (V) as, $d = (V/N)^{1/3}$. For the selected number of dipoles ($N = 1472$), the calculated lattice spacings are $d_{\min} = 1.06$ nm and $d_{\max} = 3.54$ nm for the limiting values of minimum core size ($R_c = 7.5$ nm) and maximum NP size ($R_s = 25$ nm), respectively. Hence, the nanoparticle representation with 1472 number of dipoles is enough for the lattice spacing criterion.

4. Results and discussions

The absorption efficiency (Q_{abs}) is defined as the ratio of absorption cross-section to geometrical cross-section of the targeted NP. Accurate calculation of Q_{abs} requires adequate number of dipoles. Hence, the spectral absorption behaviour of specified core–shell nanoparticle being placed on BK7 glass substrate is studied with DDA-SI-v by using optimum number of dipoles ($N = 1472$) that is identified based on the converged maximum absorption efficiency values having less than 5% relative error with respect to the predicted values using $N = 7208$ dipoles. Moreover, DDA-SI-v simulations for a single NP in free space is compared with the analytical solution of Mie theory and the other DDA method, DDSCAT. The relative errors for the simulations are estimated as 6.3% and 4.1% when the maximum absorption efficiency values are compared against DDSCAT and the Mie theory, respectively. In both validation and verification studies of DDA-SI-v, the LSPR peak wavelengths are estimated with a relative error less than 5%.

After identifying the adequate number of dipoles, TE polarization of an EM wave is studied to identify the highest absorption efficiency value. The simulations are carried out based on the specified light spectrum range (300–800 nm). For each dielectric-metal and metal-dielectric core–shell NPs, there are two cases considered, one with fixed core (FC) and varying shell thickness, and one with fixed NP (FNP) size with varying core diameter. For both cases, a common metric is defined as volumetric filling ratio, f_r, as stated in section 2. This dimensionless ratio is in the range of 0–1 and it represents the core occupancy with respect to the overall NP volume. As the filling ratio increases in the FC case, the thickness of the shell material is decreased with

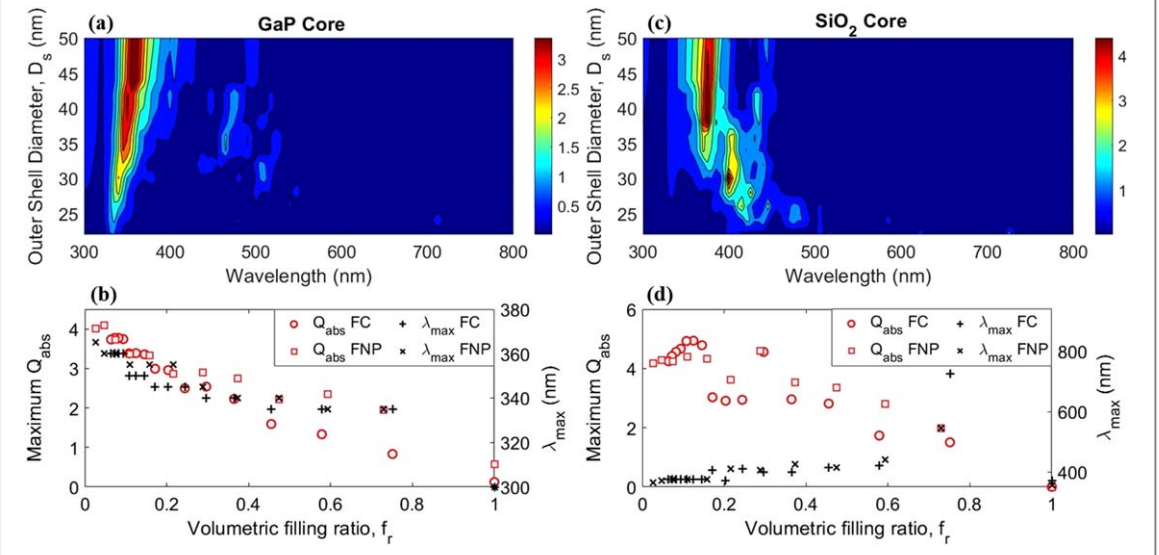


Figure 2. Ag shell with GaP (a), (b) and SiO_2 (c), (d) core: contour plots of absorption efficiency as a function of wavelength for FC (a), (c). Maximum Q_{abs} and LSPR wavelengths, λ_{max}, as function of f_r for FC and FNP (b), (d).

decreasing NP size. Similarly, an increase in core size results in increasing filling ratio, while the NP size is fixed in the FNP case.

The following two sections are the results of dielectric-metal and metal-dielectric core–shell pairs and their spectral LSPR response with respect to size configurations. The scatter plots are designated to label the first maximum LSPR peak wavelengths with corresponding absorption efficiency values, Q_{abs}, as a function of f_r. The contour plots of absorption efficiencies with respect to size and wavelength are only shown for the FC case. The effect of the core size on the range of the LSPR wavelengths is also discussed in the sections in order to compare the range of tunability of the dielectric-metal pairs. Further analysis is carried out for selected core–shell NPs, which are SiO_2 core-Au shell and Au core-GaP shell, with their normalized field intensities for different core diameters. The effect of core size on the EM field localizations is shown for these selected core–shell NPs, while the overall NP diameter is kept at 50 nm.

4.1. Dielectric core with metal shell

For this case, the results are depicted from figures 2–4. The absorption profiles of GaP core-Ag shell for both FC and FNP cases show a linear relation with respect to f_r of the GaP core. Figure 2(a) shows the maximum absorption efficiency values located near the LSPR wavelength of the bare Ag NP, which is around 365 nm. In this contour plot, apart from the first absorption maxima locations, the secondary peaks of LSPR response can be seen in cases with the outer shell diameter between 30–40 nm. In this range, hybrid modes with multipeak LSPR wavelengths are observed. Similar multipeak response is observed for the FNP case when the core diameter is between 25–35 nm. In this scenario, the primary LSPR wavelength supports EM field localizations both at the GaP core and the outer shell surface. Since the GaP has only the real part of the refractive index for the wavelengths longer than 490 nm, the secondary plasmonic mode causes field localizations at core–shell interface and on Ag shell surface when the LSPR wavelength exceeds 490 nm.

As shown in figure 2(b) for the fixed GaP core size, decreasing the f_r by increasing the Ag shell thickness results in a significant increase in the absorption efficiency from 0.83 to 3.77, while the corresponding LSPR wavelengths redshift from 335 nm to 360 nm. Similar response is observed in the FNP case with the increase of absorption efficiency from 1.95 to 4.09 and the total redshift from 335 nm to 365 nm when the GaP core size is decreased. It can be deduced that for both FC and FNP cases, increasing the f_r of the GaP core results in decreasing Q_{abs} with a blueshift of LSPR wavelength. When the f_r of the GaP core is increased, the field localization takes place on the outer surface of the Ag shell. Therefore, the NP with dielectric GaP core with relatively thinner absorbing shell material has smaller maximum absorption efficiency values.

The second case of the Ag shell is presented in figures 2(c) and (d) with SiO_2 core material, which has larger redshift than the case with GaP core. In figure 2(d), an increase of f_r of the SiO_2 core is shown with total redshifts by 355 nm and 180 nm for FC and FNP cases, respectively. Silica core having f_r greater than 30% results in decreasing absorption with a redshift in LSPR response. However, the absorption efficiencies and the LSPR wavelengths have no linear relation with the f_r. Moreover, comparison of the absorption efficiency values with the bare Ag NP with 50 nm diameter, which has maximum Q_{abs} value of 4.54 at 365 nm, showed that absorption

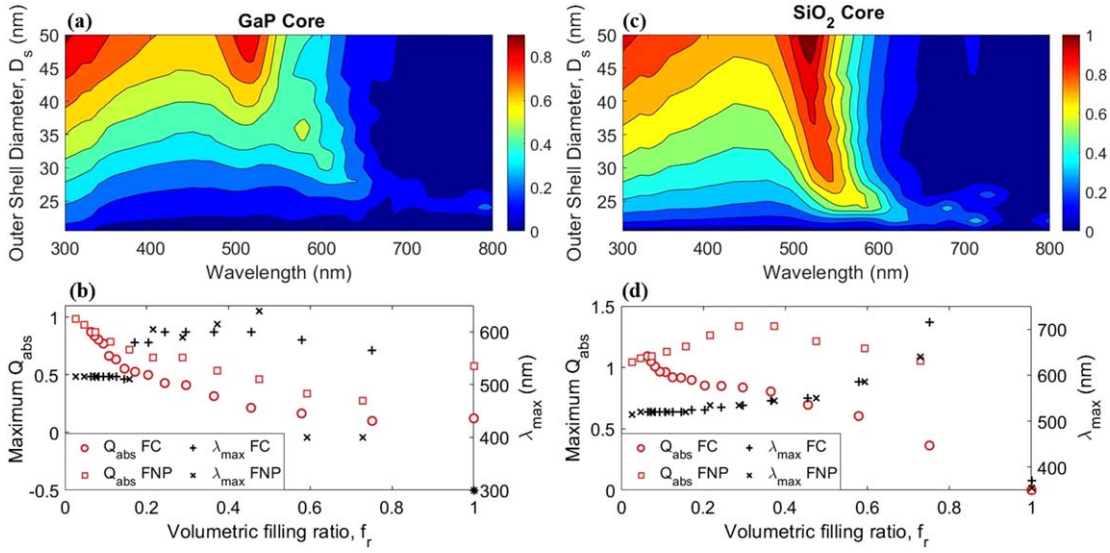


Figure 3. Au shell with GaP (a), (b) and SiO_2 (c), (d) core: contour plots of absorption efficiency as a function of wavelength for FC (a), (c). Maximum Q_{abs} and LSPR wavelengths, λ_{max}, as function of f_r for FC and FNP (b), (d).

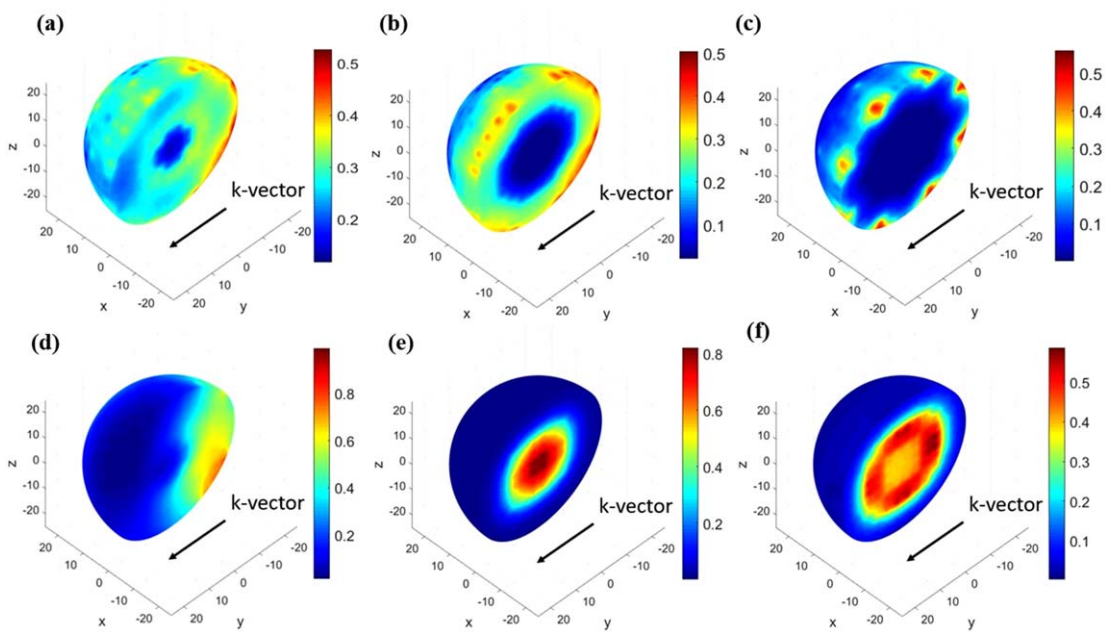


Figure 4. Normalized field intensity plots for SiO_2 core/Au shell (a)–(c) and Au core/GaP shell (d)–(f) NPs with a cut on x = 0 plane and $D_s = 50$ nm. Each case is shown with respect to k-vector direction. (a) $D_c = 15$ nm, $\lambda_{max} = 515$ nm, maximum $Q_{abs} = 1.04$. (b) $D_c = 33$ nm, $\lambda_{max} = 535$ nm, maximum $Q_{abs} = 1.34$. (c) $D_c = 45$ nm, $\lambda_{max} = 640$ nm, maximum $Q_{abs} = 1.06$. (d) $D_c = 15$ nm, $\lambda_{max} = 300$ nm, maximum $Q_{abs} = 0.58$. (e) $D_c = 27$ nm, $\lambda_{max} = 705$ nm, maximum $Q_{abs} = 1.12$. (f) $D_c = 33$ nm, $\lambda_{max} = 660$ nm, maximum $Q_{abs} = 1.61$.

enhancement of 8.81% is possible. The maximum absorption efficiency is found as 4.94 at 375 nm when the f_r of SiO_2 core is 12.5% with 10 nm Ag shell as can be seen in figure 2(d). For the NP diameter between 40–50 nm as shown in figure 2(c), secondary peak regions can be observed because the shell thickness starts exceeding the skin depth (12 nm). Moreover, in these ranges, where the f_r of the dielectric core is below 20%, most of the absorption takes place within the shell material. In the figures 2(b) and (d), both core–shell structures have LSPR wavelength patterns converging to 365 nm as the f_r of the dielectric core decreases, and Ag shell starts to dominate the plasmon response. Comparing Ag shell with dielectric core cases showed that wide tunability can be achieved with SiO_2 core, which redshifts the LSPR wavelength from the ultraviolet (UV) to the near-infrared (NIR) region of the light spectrum. However, wide tunability of LSPR response is not achieved when the core is GaP due to its non-zero imaginary part of refractive index, k, for the wavelengths smaller than 490 nm.

The absorption efficiency patterns for FC and FNP cases of the Au shell with GaP are presented in figures 3(a) and (b), which show a wide range of tunability with small secondary peak regions. We observe that the LSPR wavelength values stay constant with decreasing absorption efficiency when the f_r of the GaP core increases up to 15%, for both FC and FNP cases. As shown in figure 3(a), further increase of the f_r shows that first peak values of LSPR wavelength redshift to 570 nm whilst the non-absorbing core reduces the absorption efficiency of the NP. There is a limiting f_r value for the core resulting in blueshift of the first LSPR wavelength when it is greater than 50%.

From the figures 2(b) and 3(b), it can be observed that GaP core with the Au shell has large tunability with the range of 400–640 nm where the LSPR wavelength of the bare Au NP stays in between. On the contrary, the tunability of GaP core with Ag shell has narrower range of 335–365 nm that cannot go beyond the LSPR wavelength of the bare Ag NP (365 nm). Although GaP core with Au shell provides larger tunability of the LSPR wavelength, its absorption efficiency values are below the ones with the Ag shell.

The absorption profiles of SiO_2 core with Au and Ag shell cases shown in figures 2(d) and 3(d) reveal that increasing f_r of the core after 0.2 results in a redshift of LSPR wavelength. Figure 3(d) depicts total redshift of LSPR wavelengths of 195 nm and 125 nm for FC and FNP cases, respectively. Due to the hybrid structure of the NP, secondary peaks similar to the case of GaP core-Au shell can be observed in figure 3(c) for SiO_2 core-Au shell. Contrary to SiO_2 core-Ag shell case, maximum absorption efficiency values of SiO_2 core-Au shell has a smoother trend with respect to the f_r, as shown in figure 3(d). For the FC case in figure 3(d), decreasing the Au shell thickness decreases the absorption of the NP, while the LSPR wavelengths increase. Similar LSPR shift is observed in the FNP case with the maximum absorption efficiency values being enhanced to 1.34 at 535 nm wavelength when the f_r of the core is 30%.

As shown in figures 4(a)–(c), the EM field localizations takes place between the core–shell interface and the outer surface of the metal shell. The case in figure 4(b) shows the field intensity localizations in detail. Increasing the SiO_2 core size results in high energy confinements distributed evenly in thin shell structure while the LSPR wavelength of the NP redshifts from 515 nm to 640 nm. Moreover, compared to bare Au NP, maximum absorption efficiency is enhanced by 30% with SiO_2 core-Au shell case. Further increase of dielectric core volume for FNP case shows decreasing maximum Q_{abs} values, which are still larger than the absorption efficiency of bare Au NP with 50 nm diameter.

It is observed that SiO_2 core with Au and Ag shell cases have greater maximum absorption efficiencies due to the evenly distributed field localizations in the metal shells by comparing dielectric core/metal shell cases in figures 2 and 3. However, when GaP is used at core, field localizations can be shifted to the core with a reduction of absorption efficiency of the NP.

Moreover, metal shell domination is observed for dielectric cores with f_r values smaller than 0.2 that results in LSPR wavelengths to be located around the LSPR wavelength of the bare metallic NP. For dielectric core-metal shell pairs, it is found that increasing f_r of the core material results in a redshift of the LSPR wavelength except in GaP core-Ag shell case, which can be attributed to nonzero imaginary part of the refractive index of the GaP for the wavelength range given for this pair. Therefore, the effect of dielectric cores on the plasmonic response of these core–shell pairs cannot be generalized and these pairs should be considered individually in order to study their absorption behavior and LSPR response.

4.2. Metallic core with dielectric shell

Contrary to dielectric core-metallic shell pairs in the previous section, metallic core-dielectric shell NPs have opposite LSPR response especially for their tunability range. Comparing the figures 2(a), (b) and 5(a), (b), the total LSPR shift of the GaP/Ag pairs is observed to be greater for Ag core-GaP shell. As the f_r of Ag core decreases, LSPR wavelength of the Ag core-GaP shell shifts from 465 nm to 620 nm for FC case, and from 445 nm to 630 nm for FNP case, as shown in figure 5(b). Compared to the LSPR wavelength of the bare Ag NP, redshift of LSPR wavelength is observed for both FC and FNP cases of Ag core-GaP shell NP. Moreover, absorption enhancement of 4% can be achieved if Ag is at core rather than being at shell when it is paired with GaP. For both FC and FNP cases, almost 60% f_r of the Ag core leads to the highest absorption efficiency values. While the maximum absorption efficiency of single Ag NP with 50 nm diameter is 4.54 at 365 nm, the maximum absorption efficiency is found to be 4.74 at 510 nm for the Ag core-GaP shell with FNP case in figure 5(b). Hence it is possible to use Ag core-GaP shell for enhanced absorption with a redshifted LSPR wavelength. The absorption profiles of Ag core-GaP shell in figure 5(b) for both FC and FNP cases exhibit similar pattern with respect to f_r. Decreasing the f_r of the Ag core results in LSPR wavelength shifting from 365 nm to longer wavelengths. Contrary to GaP core-Ag shell case, where increasing the GaP core results in blueshift of LSPR wavelengths, increasing the GaP shell volume relative to the Ag core provides a redshift of LSPR. This opposite LSPR response is due to the increasing dielectric constant of the surrounding medium of Ag with the introduction of GaP shell.

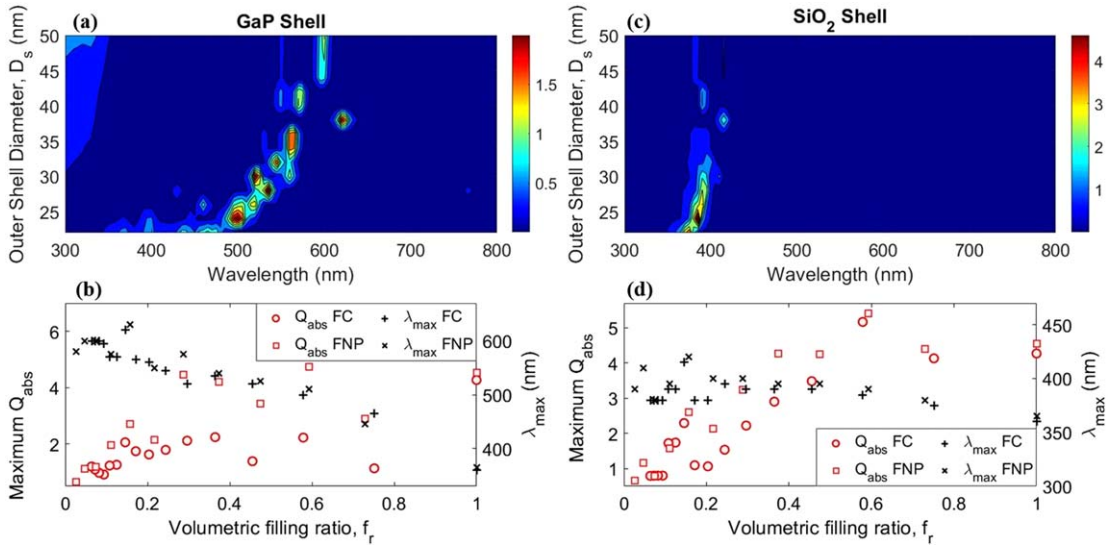


Figure 5. Ag core with GaP (a), (b) and SiO_2 (c), (d) shell: contour plots of absorption efficiency as a function of wavelength for FC (a), (c). Maximum Q_{abs} and LSPR wavelengths, λ_{max}, as function of f_r for FC and FNP (b), (d).

Similar to the GaP/Ag pairs, the LSPR responses of SiO_2/Ag pairs show different phenomenon, when the core and shell materials are switched. As shown in figures 5(c) and (d) the range of LSPR wavelengths of Ag core-SiO_2 shell is narrower as compared to the ones in SiO_2 core-Ag shell case being presented in figures 2(c) and (d). For both FC and FNP cases, changing the f_r of Ag core results in only 40 nm change of LSPR wavelength. There is an obvious trade-off between the absorption enhancement and LSPR wavelength with the tunability of the NP.

As stated in dielectric core-metal shell section, SiO_2 core-Ag shell can have absorption enhancement of 8.81% with 355 nm of LSPR wavelength shift in FC case. However, when the core and shell are switched to Ag and SiO_2, respectively, absorption enhancement of 19% is obtained with an absorption efficiency of 5.40 and 25 nm redshift of LSPR wavelength.

As shown in figures 5(c) and (d), decreasing the f_r of the Ag to 30% results in a redshift of LSPR peak wavelengths. Further decrease in the f_r of the Ag core with both GaP and SiO_2 dielectric shell cases, shell starts to dominate over the plasmon response with damping of absorption and fluctuating LSPR wavelengths.

For the GaP core-Au shell being shown in figures 3(a) and (b), maximum absorption efficiency of the NP is below 1 with LSPR wavelength at 515 nm. However, when Au core-GaP shell pair is investigated, maximum absorption efficiency is obtained as 1.61 at 660 nm of LSPR wavelength with 30% f_r of the Au core in the FNP case, as shown in figures 4(f) and 6(b). Considering bare Au NP having maximum absorption efficiency of 1.03 at 515 nm wavelength, GaP shell with Au core can both enhance the absorption up to 56% and redshift the LSPR wavelength by 145 nm. Moreover, tunability of LSPR wavelength is greater than the case with GaP core-Au shell. As shown in figures 6(a) and (b), decreasing Au core f_r results in LSPR wavelengths being shifted from 550 nm to 705 nm. Similar redshift effect of the increasing dielectric shell was observed with the Ag core-dielectric shell cases as the dielectric constant of the surrounding medium is increased due to the introduction of shell. As shown in figure 6(b), decreasing the f_r of the core below 30% drastically decreases the absorption efficiency as the GaP shell dominates the plasmon response of the core–shell at lower wavelengths.

As discussed in sections 2 and 4.1, the wavelengths smaller than 490 nm can induce absorption in GaP material due to its nonzero imaginary part of the refractive index, k. Hence, most of the field localization takes place on the GaP shell with LSPR wavelength of 300 nm, as shown in figure 4(d). Figures 4(e) and (f) depict increasing the Au core size, while keeping the NP diameter at 50 nm, shifts the maximum field intensity regions towards the Au core with greater absorption efficiency values. Since the LSPR wavelengths are greater than 490 nm in figures 4(e) and (f), GaP shell can act as a perfectly dielectric material, which can induce a redshift of LSPR wavelengths with an increasing shell thickness.

As shown in figure 6(a), for the FC case with the outer shell diameter between 40–50 nm, primary and secondary LSPR regions exist although the absorption is observed to be relatively low. Further decrease in the shell diameter prevents formation of the multiple peaks of the LSPR response as the Au core starts to dominate over GaP shell. Au core domination is also observed in figures 4(d)–(f) and 6(b), where the LSPR wavelengths also blueshift towards the LSPR wavelength of the bare Au NP.

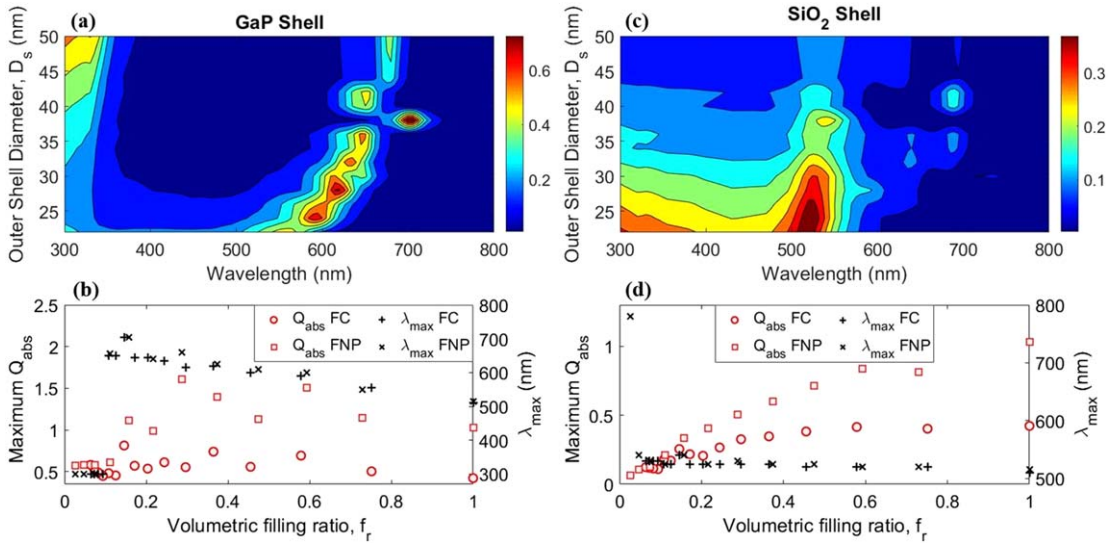


Figure 6. Au core with GaP (a), (b) and SiO_2 (c), (d) shell: contour plots of absorption efficiency as a function of wavelength for FC (a), (c). Maximum Q_{abs} and LSPR wavelengths, λ_{max}, as function of f_r for FC and FNP (b), (d).

The GaP shell extends the range of LSPR wavelengths for both metallic cores. On the other hand, the SiO_2 shell restricts the range of LSPR shifts. Comparing the figures 3(d) and 6(d) for SiO_2/Au pairs, it is observed that the shifting range of LSPR wavelengths narrows down from 195 nm to 20 nm when SiO_2 shell is used. Moreover, shielding of SiO_2 shell leads to the lower absorption efficiency values with decreasing f_r of the Au core, as shown in figure 6(d). Hence, the absorption enhancement with respect to the bare Au NP cannot be achieved with this core–shell structure.

All metallic core-dielectric shell pairs show that dielectric shell can redshift the LSPR wavelength of the NPs compared to ones for the bare Ag and Au NPs. Besides a redshift of the LSPR wavelength, there is an absorption enhancement with the introduction of dielectric shell except for the case of Au core- SiO_2 shell NPs. It is useful to choose silica shell with Ag core for selective heating applications of NPs that have enhanced absorption and chemically stable surface. The other case with Au core-GaP shell can be used for nanomanufacturing applications as they have 56% more absorption at wavelengths such as 660 nm.

5. Conclusion

Localized surface plasmon resonance (LSPR) of core–shell nanoparticle pairs are studied for their potential use in localized heating applications. Numerical analyses of core–shell pairs are carried out by using vectorized version of DDA-SI (DDA-SI-v). Optical tunability of the hybrid structures is investigated with dielectric-metal and metal-dielectric pairs. Moreover, LSPR wavelength and absorption efficiency patterns are studied through various size configurations of the core–shell structure.

When the dielectric core-metal shell cases are examined, the maximum absorption enhancement is observed in SiO_2 core-Au shell which is preferably used as local heat sources in photothermal therapies. Although the maximum absorption enhancement of the SiO_2 core is observed with Au shell case, the greatest redshift of the LSPR wavelength occurs for the Ag shell case. Contrary to SiO_2 core cases, it is shown that decreasing the metal shell thickness results in both redshift and blueshift of the LSPR wavelength for GaP core-metal shell pairs. Since there is no general conclusion for the effect of dielectric core on the LSPR wavelength response, each dielectric core material needs to be evaluated individually.

The metal core-dielectric shell cases are also good candidates for optical tuning and field enhancement. It is found that maximum LSPR wavelength shift with maximum absorption enhancement can be obtained with Au core-GaP shell. Moreover, using GaP at shell rather than at core results in both redshift of the LSPR wavelength and enhanced absorption for both Au and Ag metallic core cases. For the SiO_2 shell, maximum absorption efficiency increase is observed in Ag core case. If the shell is dielectric, then it redshifts the LSPR wavelengths since they act as a dielectric medium for the metallic cores. Hence, the hybrid structures of metal core-dielectric shell NPs can be utilized both with its enhanced absorption efficiency and with a wide range of optical tunability as compared to the bare metallic NPs.

ORCID iDs

Hakan Ertürk https://orcid.org/0000-0001-5564-3845

References

[1] Maier S A 2007 *Plasmonics: Fundamentals and Applications* (New York: Springer) (https://doi.org/10.1007/0-387-37825-1)
[2] Huda G M, Donev E U, Mengüç M P and Hastings J T 2011 Effects of a silicon probe on gold nanoparticles on glass under evanescent illumination *Opt. Express* **19** 12679
[3] Taylor J, Huefner A, Li L, Wingfield J and Mahajan S 2016 Nanoparticles and intracellular applications of surface-enhanced Raman spectroscopy *R. Soc. Chem.* **141** 5037–55
[4] Joulain K, Ben-Abdallah P, Chapuis P O, De Wilde Y, Babuty A and Henkel C 2014 Strong tip-sample coupling in thermal radiation scanning tunneling microscopy *J. Quant. Spectrosc. Radiat. Transf.* **136** 1–15
[5] McCarthy B, Zhao Y, Grover R and Sarid D 2005 Enhanced Raman scattering for temperature measurement of a laser-heated atomic force microscope tip *Appl. Phys. Lett.* **86** 1–3
[6] Lal S, Clare S E and Halas N J 2008 Nanoshell-enabled photothermal cancer therapy: impending clinical impact *Acc. Chem. Res.* **41** 1842–51
[7] Pattani V P and Tunnell J W 2012 Nanoparticle-mediated photothermal therapy: a comparative study of heating for different particle types *Lasers Surg. Med.* **44** 675–84
[8] Strobbia P, Languirand E and Cullum B M 2015 Recent advances in plasmonic nanostructures for sensing: a review *Opt. Eng.* **54** 100902
[9] Loke V L Y and Mengüç M P 2010 Surface waves and atomic force microscope probe-particle near-field coupling : discrete dipole approximation with surface interaction *J. Opt. Soc. Am. A* **27** 2293–303
[10] Hawes E A, Hastings J T, Crofcheck C and Mengüç M P 2008 Spatially selective melting and evaporation of nanosized gold particles *Opt. Lett.* **33** 1383–5
[11] Honda M, Saito Y, Smith N I, Fujita K and Kawata S 2011 Nanoscale heating of laser irradiated single gold nanoparticles in liquid *Opt. Express* **19** 12375–83
[12] Hawes E A, Hastings J T, Crofcheck C and Mengüç M P 2007 Spectrally selective heating of nanosized particles by surface plasmon resonance *J. Quant. Spectrosc. Radiat. Transf.* **104** 199–207
[13] Talebi Moghaddam S, Avşar D, Ertürk H and Mengüç M P 2017 Effect of the probe location on the absorption by an array of gold nanoparticles on a dielectric surface *J. Quant. Spectrosc. Radiat. Transf.* **197** 106–13
[14] Rostampour Fathi Z, Mengüç M P and Ertürk H 2018 Plasmon coupling between complex gold nanostructures and a dielectric substrate *Appl. Opt.* **57** 8954–63
[15] Zhou H S, Honma I, Komiyama H and Haus J W 1994 Controlled synthesis and quantum-size effect in gold-coated nanoparticles *Phys. Rev.* B **50** 12052–6
[16] Talebi Moghaddam S, Ertürk H and Mengüç M P 2016 Enhancing local absorption within a gold nano-sphere on a dielectric surface under an AFM probe *J. Quant. Spectrosc. Radiat. Transf.* **178** 124–33
[17] Hirsch L R, Stafford R J, Bankson J A, Sershen S R, Rivera B, Price R E, Hazle J D, Halas N J and West J L 2003 Nanoshell-mediated near-infrared thermal therapy of tumors under magnetic resonance guidance *Proc. Natl. Acad. Sci.* **100** 13549–54
[18] Sathiyamoorthy K and Kolios M C 2015 Numerical investigation of plasmonic properties of gold nanoshells *Proc. SPIE* **9340** 93400V
[19] Oldenburg S J, Averitt R D, Westcott S L and Halas N J 1998 Nanoengineering of optical resonances *Chem. Phys. Lett.* **288** 243–7
[20] Prodan E, Radloff C, Halas N J and Nordlander P 2003 A hybridization model for the plasmon response of complex nanostructures *Science* **302** 419–22
[21] Wang Y, Qian W, Tan Y and Ding S 2008 A label-free biosensor based on gold nanoshell monolayers for monitoring biomolecular interactions in diluted whole blood *Biosens. Bioelectron.* **23** 1166–70
[22] Park H S, Kim J Y, Kim M W, Cho Y H and Kwon M K 2017 Localized surface plasmon-enhanced emission from red phosphor with Au–SiO_2 nanoparticles *Mater. Lett.* **205** 145–9
[23] Yu P, Yao Y, Wu J, Niu X, Rogach A L and Wang Z 2017 Effects of plasmonic metal core-dielectric shell nanoparticles on the broadband light absorption enhancement in thin film solar cells *Sci. Rep.* **7** 1–10
[24] Riva E R, Desii A, Sinibaldi E, Ciofani G, Piazza V, Mazzolai B and Mattoli V 2014 Gold nanoshell/polysaccharide nanofilm for controlled laser-assisted tissue thermal ablation *ACS Nano* **8** 5552–63
[25] Purcell E M and Pennypacker C R 1973 Scattering and absorption of light by nonspherical dielectric grains *Astrophys. J.* **186** 705–14
[26] Draine B T and Flatau P J 1994 Discrete-dipole approximation for scattering calculations *J. Opt. Soc. Am.* A **11** 1491–9
[27] Draine B T and Flatau P J 2008 Discrete-dipole approximation for periodic targets: theory and tests *J. Opt. Soc. Am.* A **25** 2693–703
[28] Yurkin M A and Hoekstra A G 2011 The discrete-dipole-approximation code ADDA: capabilities and known limitations *J. Quant. Spectrosc. Radiat. Transf.* **112** 2234–47
[29] Loke V L Y, Mengüç M P and Nieminen T A 2011 Discrete-dipole approximation with surface interaction: computational toolbox for MATLAB *J. Quant. Spectrosc. Radiat. Transf.* **112** 1711–25
[30] Short M R, Geffrin J M, Vaillon R, Tortel H, Lacroix B and Francoeur M 2014 Evanescent wave scattering by particles on a surface: validation of the discrete dipole approximation with surface interaction against microwave analog experiments *J. Quant. Spectrosc. Radiat. Transf.* **146** 452–8
[31] Loke V L Y, Huda G M, Donev E U, Schmidt V, Hastings J T, Mengüç M P and Wriedt T 2014 Comparison between discrete dipole approximation and other modelling methods for the plasmonic response of gold nanospheres *Appl. Phys. B Lasers Opt.* **115** 237–46
[32] Albella P, De La Osa R A, Moreno F and Maier S A 2014 Electric and magnetic field enhancement with ultralow heat radiation dielectric nanoantennas: considerations for surface-enhanced spectroscopies *ACS Photonics* **1** 524–9
[33] Cambiasso J, Grinblat G, Li Y, Rakovich A, Corte E and Maier S A 2017 Bridging the gap between dielectric nanophotonics and the visible regime with effectively lossless gallium phosphide antennas *ACS Nano Lett.* **17** 1219–25
[34] Johnson P B and Christy R W 1972 Optical constants of the noble metals *Phys. Rev. B* **6** 4370–9
[35] Aspnes D E and Studna A A 1983 Dielectric functions and optical parameters of Si, Ge, GaP, GaAs, GaSb, InP, InAs, and InSb from 1.5 to 6.0 eV *Phys. Rev.* B **27** 985–1009